This article has been accepted for publication in a future issue of this journal, but has not been fully edited. Content may change prior to final publication. Citation information: DOI 10.1109/JESTPE.2014.2313185, IEEE Journal of Emerging and Selected Topics in Power Electronics

A Single-Stage Three-Phase Inverter Based on Cuk Converters for PV Applications

A. Darwish, D. Holliday, S. Ahmed, *Senior Member, IEEE*, A. M. Massoud, *Senior Member, IEEE*, and B. W. Williams

***Abstract* -- This paper presents a new three-phase inverter based on the Cuk converter. The main feature of the proposed topology is that the energy storage elements such as inductors and capacitors, can be reduced in order to improve the reliability, reduce the size, and the total cost. The buck-boost inherent characteristic of the Cuk converter, depending on the time-varying duty ratio, provides flexibility for stand-alone and grid connected applications when the required output ac voltage is lower or greater than the dc side voltage. This property is not found in the conventional current source inverter when the dc input current is always greater than the ac output or in the conventional voltage source inverter as the output ac voltage is always lower than the dc input. The proposed system allows much smaller, more reliable non-electrolytic capacitors to be used for energy source filtering. The new three-phase inverter is convenient for PV applications where continuous input currents are required for maximum power point tracking operation. Average large and small signal models are used to study the Cuk converter's nonlinear operation. The basic structure, control design, and MATLAB/SIMULINK results are presented. Practical results substantiate the design flexibility of the Cuk based topology controlled by a TMSF280335 DSP.**

Index terms — DC/DC converters, Cuk converter, buck-boost inverter, state space averaging, PI control, PR control, switched mode power supply

NOMENCLATURE

*	Reference value of a variable
abc	Three-phase stationary frame
C_1	Cuk converter capacitor
d	Cuk converter instantaneous duty ratio
d-q	Direct and quadrature synchronous frame
f	Output voltage fundamental frequency
f_s	Sampling frequency
H_{ac}	ac voltage ratio
H_{dc}	dc voltage ratio
I_{in}	Total input current
I_{L1}	Cuk converter input current
I_{L2}	Cuk converter output current
I_o	Peak value of load three-phase current
L_1, L_2	Cuk converter input and output inductors
T_s	Sampling time
V_{c1}	Cuk capacitor voltage
V_{c2}	Cuk output voltage
V_{in}	Cuk input voltage
V_o	Output load three-phase voltage
Z	Load impedance
γ	Phase angle of load three-phase current
δ	Steady state Cuk converter duty ratio
θ	Phase angle of Cuk three-phase voltage

I. INTRODUCTION

THERE is a trend toward modular structured renewable/distributed system concepts in order to reduce costs and provide high reliability [1]. This trend affects dc-ac converter topologies significantly in terms of reducing the size and number of inverter passive components [2]. For dc-to-ac conversion, the conventional voltage source inverter (VSI) is the most common converter topology [3]. The instantaneous average output voltage of the VSI is always lower than the input dc voltage. For this reason, a boost dc-dc converter is needed when the required ac peak output voltage is greater than the input dc voltage [4]. This additional dc-dc boost converter increases volume, weight, cost, and losses and decreases reliability [5]. In [3], a new boost inverter is presented where the required output voltage can be lower or greater than the input dc voltage by connecting the load differentially across two dc–dc converters and modulating the converter output voltages sinusoidally. Both individual boost converters are driven by two 180° phase-shifted dc-biased sinusoidal references. The differential connection of the load leads to cancellation of the dc offsets from the output voltage and the peak ac voltage can be lower or greater than the dc input voltage. The main drawback of this structure is its control; as ac output voltage control requires control of both boost converters, hence the load voltage is controlled indirectly and large capacitances are connected across the output. In [6], a closed-loop sinusoidal PWM-PID control method with real-time waveform feedback is presented. In [7], the simulation of a hybrid boost inverter control system is proposed in order to highlight the dc offset error. The topologies of buck, boost, and buck-boost inverters are presented in [8]. In [9], the boost-inverter topology is used to build a single-phase single power stage fuel cell system with a backup battery storage unit. Four switches and four diodes are used as well as two output capacitors for each phase. In [10], the authors propose parallel operation of a three-phase ac to dc converter using a single-phase rectifier module. The control strategy has good dynamic features, giving a fast dynamic transient response. However, the proposed configuration includes six Cuk converters with six rectifiers: two single-switch single-diode Cuk converters with two rectifiers for each phase. This all contributes to the cost, control complexity and the reliability of the overall system, in addition to the use of high capacitance across the load. In [11], the authors presented a single-phase inverter with a sliding mode control approach. The inverter consists of two converters with six switches where each of the two converters is responsible for constructing a half cycle of the load voltage and current. Reference [12] presents a 7-switches inverter

This article has been accepted for publication in a future issue of this journal, but has not been fully edited. Content may change prior to final publication. Citation information: DOI 10.1109/JESTPE.2014.2313185, IEEE Journal of Emerging and Selected Topics in Power Electronics

topology where the power is transferred from dc to ac through two stages. A buck-boost converter is followed by a directing bridge. The three-phase PWM square wave current blocks from the inverter are filtered by three inductors.

For modern power conversion applications, continuous input current converters are more attractive solutions for renewable systems, since they minimize the filtering requirements. In addition, maximum power point tracking (MPPT) techniques for photovoltaic (PV) systems require continuous PV current flow [13]–[16].

Generally, there are nine continuous input and output current switched mode power supplies (SMPS) of a total of 33 possible single-switch and single-diode dc-dc-converter. These nine converters include two inductors and one capacitor [16]. Among these converters with continuous input current, the Cuk converter has the lowest losses and the best voltage regulation. Moreover, the switched capacitor of the Cuk converter increases the voltage boost ability [16]. Because of its buck-boost capability, the Cuk converter is used widely in power electronics applications such as wind energy and PV systems, marine applications, light-emitting diode drivers, compressors, fuel cells, and batteries [17]. Much research has been conducted into the design of inverters which avoid heavy expensive line frequency transformers; instead, an SMPS such as the Cuk converter can implement boosting, with wave-shaping functionality [17]-[20]. In addition, small and light weight high frequency isolation transformers can be integrated into the SMPS design if isolation and a greater voltage conversion range are required. Moreover, the output current sourcing nature of Cuk converter enables easy parallel connection and this is a trend for paralleling numerous PV arrays to the same point of common coupling (PCC). Cuk converter dc-dc operation has been studied and reported extensively in the literature. Open and closed loop stability is considered in [21]. Generally, dc-dc converters, including the Cuk converter, are time-variant systems. This means that the overall converter transfer function describing the input-output performance is dependent on the duty ratio as well as converter parameters. This increases control design complexity as the converter poles and zeros travel through a specified trajectory. Also the time-varying transfer function leads to output voltage and current distortion [22]. This paper proposes a new three-phase inverter based on three bidirectional two-switch two-diode Cuk converters with an optional small dc-link capacitor and describes an appropriate and practical control structure that can be used efficiently in industry applications. The proposed inverter is expedient for PV applications where the peaks of the output ac currents are required to be flexible over and below the input dc current for MPPT operation and for providing easy paralleling at the PCC.

II. System Description

The operating modes of a Cuk converter are shown in Fig. 1. The circuitry consists of an input voltage source V_{in}, two switches S_1 and S_2, two antiparallel diodes D_1 and D_2. The energy between the voltage source and the load is transferred through capacitor C_1. The energy is stored instantaneously in inductors L_1 and L_2.The basic operation at steady state can be described simply, when S_1 is OFF, C_1 is charged leading I_{L1} to decrease while $L_2$is discharged in the load causing I_{L2} to increase. At the next switching period, when S_1 is ON, L_1 is charged and I_{L1} increases while C_1 is discharged causing $I_{L2}$to increase. It can be deduced that I_{L1} and I_{L2} are interrelated via the energy transfer through C_1.

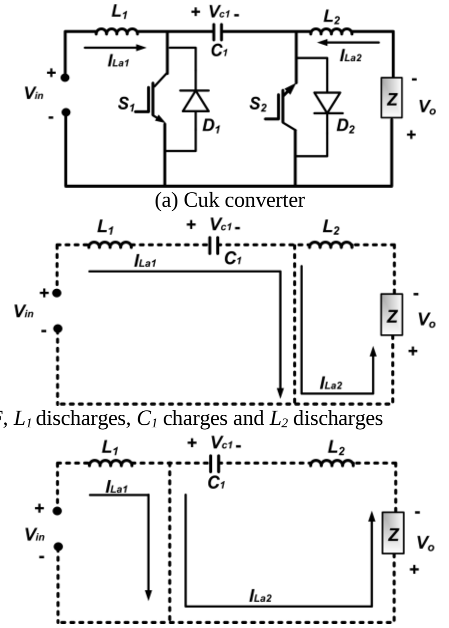

(a) Cuk converter

(b) S_1 = OFF, L_1 discharges, C_1 charges and L_2 discharges

(c) S_1 = ON, L_1 charges, C_1 discharges and L_2 charges

Fig. 1 The operating modes of a typical Cuk converter

The state space averaging method will be used to model the Cuk converter. Assuming the turn off time of S_1 is T_{off}, turn on time for S_1 = ON is T_{on} and $T_s = T_{on} + T_{off}$, the state space equations during a continuous conduction mode of operation can be written as:

i) S_1 *OFF and* S_2 *ON* $(0 < t < T_{off})$

$$\frac{di_{L1}}{dt} = \frac{1}{L_1}V_{in} - \frac{1}{L_1}v_{c1} \tag{1a}$$

$$\frac{dv_{c1}}{dt} = \frac{1}{C_1}i_{L1} \tag{1b}$$

$$\dot{x}_1 = A_1 x_1 + B_1 V_{in} \tag{1c}$$

$$v_{o1} = Y_1 x_1 \tag{1d}$$

$$A_1 = \begin{bmatrix} 0 & \frac{-1}{L_1} & 0 \\ \frac{1}{C_1} & 0 & 0 \\ 0 & 0 & \frac{-Z}{L_2} \end{bmatrix}, B_1 = \begin{bmatrix} \frac{1}{L_1} \\ 0 \\ 0 \end{bmatrix} \tag{1e}$$

$$Y_1 = \begin{bmatrix} 0 & 0 & Z \end{bmatrix}, x_1 = \begin{bmatrix} i_{L1} & v_{c1} & i_{L2} \end{bmatrix}$$

ii) S_1 *ON and* S_2 *OFF* $(T_{off} < t < T_s)$

$$\frac{di_{L1}}{dt} = \frac{1}{L_1}V_{in} \tag{2a}$$

$$\frac{dv_{c1}}{dt} = -\frac{1}{C_1}i_{L2} \tag{2b}$$

$$\dot{x}_2 = A_2 x_2 + B_2 V_{in} \tag{2c}$$

$$v_{o2} = Y_2 x_2 \tag{2d}$$

$$A_2 = \begin{bmatrix} 0 & 0 & 0 \\ 0 & 0 & -\frac{1}{C_1} \\ 0 & \frac{1}{L_2} & \frac{-Z}{L_2} \end{bmatrix}, B_2 = \begin{bmatrix} \frac{1}{L_1} \\ 0 \\ 0 \end{bmatrix} \tag{2e}$$

$$Y_2 = \begin{bmatrix} 0 & 0 & Z \end{bmatrix}, x_2 = \begin{bmatrix} i_{L1} & v_{c1} & i_{L2} \end{bmatrix}$$

Averaging the state space equations over the period $[0 < t < T_s]$ assuming the duty ratio $d = \frac{T_{on}}{T_s}$

$$\begin{aligned} A &= A_1(1-d) + A_2 d \\ B &= B_1(1-d) + B_2 d \\ Y &= Y_1(1-d) + Y_2 d \end{aligned} \tag{3a}$$

$$\begin{aligned} \dot{x} &= Ax + BV_{in} \\ v_o &= Yx \end{aligned} \tag{3b}$$

$$A = \begin{bmatrix} 0 & \frac{-(1-d)}{L_1} & 0 \\ \frac{(1-d)}{C_1} & 0 & -\frac{d}{C_1} \\ 0 & \frac{d}{L_2} & \frac{-Z}{L_2} \end{bmatrix}, B = \begin{bmatrix} \frac{1}{L_1} \\ 0 \\ 0 \end{bmatrix} \tag{3c}$$

$$Y = \begin{bmatrix} 0 & 0 & Z \end{bmatrix}, x = \begin{bmatrix} i_{L1} & V_{c1} & i_{L2} \end{bmatrix}$$

From 3c, the voltage transfer function of the Cuk converter $[G_v = \frac{V_o}{V_{in}}]$ can be written as:

$$G_v = \frac{Zd(1-d)}{C_1 L_1 L_2 s^3 + C_1 L_1 Z s^2 + s(L_2 - 2dL_2 + d^2 L_2) + (Z - 2Zd + d^2 Z)} \tag{3d}$$

From 3d, the dynamics of output voltage depends on the duty ratio d. At steady state, ($s \to 0$) and when $d = \delta$ is constant, the transfer function tends to:

$$G_{v,ss} = \frac{\delta}{1-\delta} \tag{3e}$$

In the same approach, the current transfer function $G_i = \frac{I_{L2}}{I_{L1}}$ can be obtained as:

$$\begin{aligned} G_i &= \frac{d(1-d)}{C_1 L_1 s^2 + s(C_1 Z) + d^2} \\ G_{i,ss} &= \frac{1-\delta}{\delta} = \frac{1}{G_{v,ss}} \end{aligned} \tag{3f}$$

The proposed three-phase inverter based on Cuk converters is shown in Fig. 2. As a current source, the proposed system can be paralleled for any further power extension. Each Cuk converter builds a sinusoidal output voltage, specifically current, with a dc-offset. Assuming that the dc and ac voltages ratios between output and input are H_{dc} and H_{ac} respectively, (4) explains the relation between the input and output voltage:

$$\begin{aligned} V_{c2a} &= H_a V_{in} \\ H_a &= H_{dc} + H_{ac} \sin(\omega t + \theta) \end{aligned} \tag{4a}$$

$$\begin{aligned} V_{c2b} &= H_b V_{in} \\ H_b &= H_{dc} + H_{ac} \sin(\omega t - \frac{2\pi}{3} + \theta) \end{aligned} \tag{4b}$$

$$\begin{aligned} V_{c2c} &= H_c V_{in} \\ H_c &= H_{dc} + H_{ac} \sin(\omega t + \frac{2\pi}{3} + \theta) \end{aligned} \tag{4c}$$

$$\delta_a = \frac{H_a}{H_a + 1},\ \delta_b = \frac{H_b}{H_b + 1} \text{ and } \delta_c = \frac{H_c}{H_c + 1} \tag{4d}$$

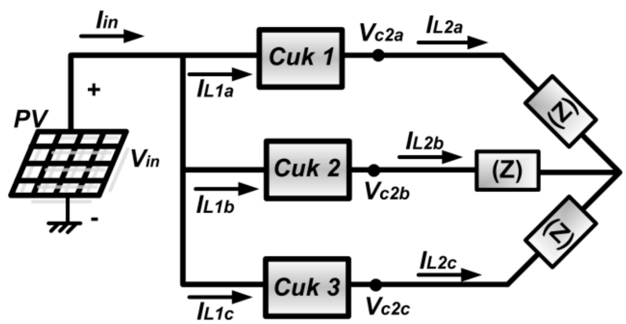

Fig. 2. Proposed Cuk-based three-phase Inverter

$$\begin{aligned} I_{L2a} &= \frac{2}{3Z} V_{c2a} - \frac{1}{3Z} V_{c2b} - \frac{1}{3Z} V_{c2c} \\ &= I_o \sin(\omega t + \gamma) \end{aligned} \tag{5a}$$

$$\begin{aligned} I_{L2b} &= -\frac{1}{3Z} V_{c2a} + \frac{2}{3Z} V_{c2b} - \frac{1}{3Z} V_{c2c} \\ &= I_o \sin(\omega t - \frac{2\pi}{3} + \gamma) \end{aligned} \tag{5b}$$

$$\begin{aligned} I_{L2c} &= -\frac{1}{3Z} V_{c2a} - \frac{1}{3Z} V_{c2b} + \frac{2}{3Z} V_{c2c} \\ &= I_o \sin(\omega t + \frac{2\pi}{3} + \gamma) \end{aligned} \tag{5c}$$

Because of the balanced energy operation of the three phases, it is predictable that the dc offsets of each phase are cancelled and the three-phase load encounters pure sinusoidal voltages and currents as described in (5). The operation of each Cuk converter for each sampling period T_s is shown in Fig. 3. Assuming that too short T_s lead to a linear energy transfer; the relation of the ripple I_{L1} and I_{L2} with L_1 and L_2 when S_1 is on, can be described as in (6):

$$\begin{aligned} V_{in} &= L_1 \frac{\Delta I_{L1}}{\Delta t} \\ L_1 &= \frac{V_{in}\,\delta}{\Delta I_{L1}\, f_s} \end{aligned} \tag{6a}$$

$$\begin{aligned} V_o &= L_2 \frac{\Delta I_{L2}}{\Delta t} \\ L_2 &= \frac{V_o\,\delta}{\Delta I_{L2}\, f_s} \end{aligned} \tag{6b}$$

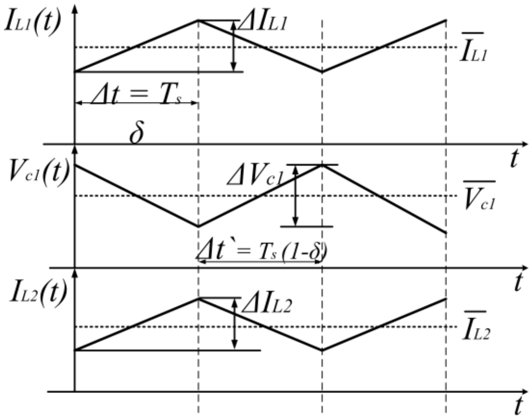

Fig. 3. Cuk converter operation

Using the same approach and neglecting the small change in I_{L2}, the ripple of C_1 can be calculated when S_2 is on:

$$\bar{I}_{L2} = C_1 \frac{\Delta V_{c1}}{\Delta t`}$$
$$C_1 = \frac{(1-\delta)}{\Delta V_{c1}\, f_s} \bar{I}_{L2} \qquad (6c)$$

where $\bar{I}_{l2}$ in (6c) is the average output current over the sampling period T_s. From the previous analysis, the highest ΔI_{L1}, ΔI_{L2} and ΔV_{c1} occur at the largest δ of each converter. Acceptable values of the system ripple as well as the peak values of the converter rated currents and voltages will determine the values of L_1, L_2 and C_1. Here, $L_1 = L_2 =$ 1mH and C_1 = 10μF are chosen based on the rated values in Table I and (6).

Table. I. Rated values

Parameter	Value
V_{in}	50 Vdc
I_{in}	50 A
$V_o(peak)$	50 Vac
$I_{L2}(peak)$	33.33 A
Z	1.5 Ω
δ_{min} and δ_{max}	0 and 0.667
f_s	50 kHz
ΔI_{L1}	0.667 A
ΔI_{L2}	0.667 A
ΔV_{c1}	20 V

Fig. 4 shows the open loop performance of the system in Fig. 2 with the parameters in Table I and 10nF optional output shunt capacitors. The expected output voltages at points V_{c2a}, V_{c2b} and V_{c2c} are sinusoidal voltages of magnitude 50V peak and 50V dc offset. The duty ratios of the three Cuk converters, δ_a, δ_b and δ_c are calculated from H_a, H_b and H_c as explained in (6) and are shown in Fig. 4a and b, respectively. However, the output voltages in Fig. 4c are distorted. From the output currents in Fig. 4d and their components in the d-q synchronous rotating frame in Fig. 4e that a 2nd harmonic component appears because of the Cuk non-linear nature. For the parameters shown in Table I, the poles and zeros of G_v are derived and plotted in Fig. 5a in order to study the dynamic behavior. The duty ratio is varied from 0.1 to 0.85. It can be concluded that increasing the duty ratio, leads the dominant poles of the real axis to move to the slower region, towards the origin, and the system dynamics become slower. This can be verified from the step response in Fig. 5b as the system gets slower with increasing duty ratio. To show the meaning of the previous analysis, a MATLAB simulation is used when the duty ratio is varied according to G_v to draw a sinusoidal output voltage with a dc offset. The input voltage is set to 50V. Fig. 5c shows the difference between the reference and the actual output voltages because of the variation of dynamics with the value of duty ratio. In the next section, a control strategy is proposed to deal with the nonlinearity, control the desired output current, and eliminate the predefined distortion.

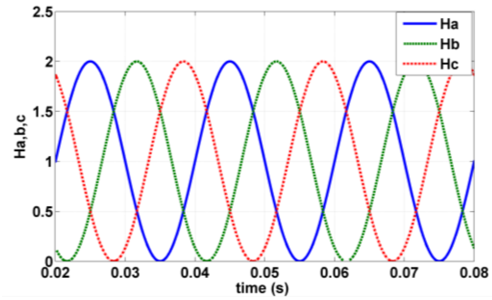

(a) $H_{a,b,\ and\ c}$

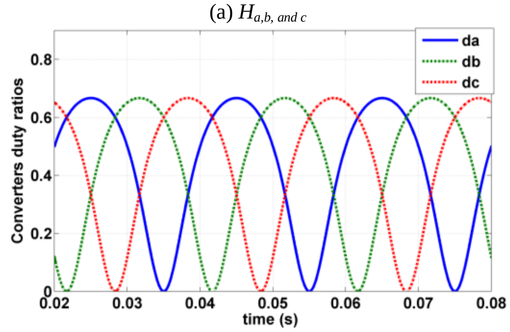

(b) Duty ratios

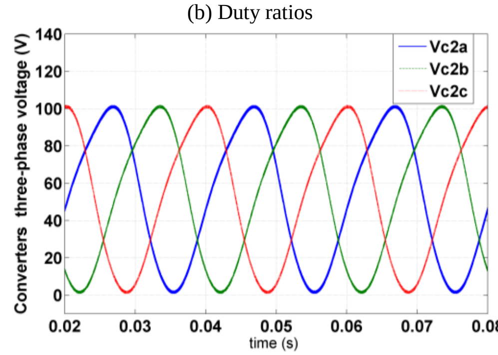

(c) Output voltages at V_{c2a}, V_{c2b} and V_{c2c}

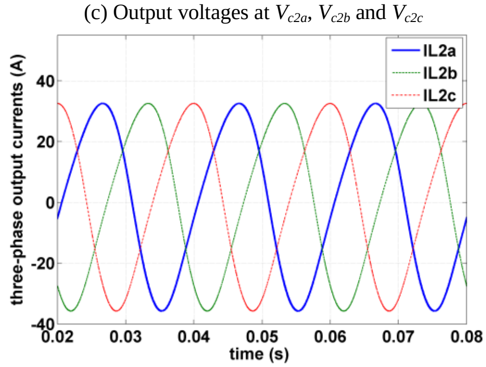

(d) Three-phase Output currents

This article has been accepted for publication in a future issue of this journal, but has not been fully edited. Content may change prior to final publication. Citation information: DOI 10.1109/JESTPE.2014.2313185, IEEE Journal of Emerging and Selected Topics in Power Electronics

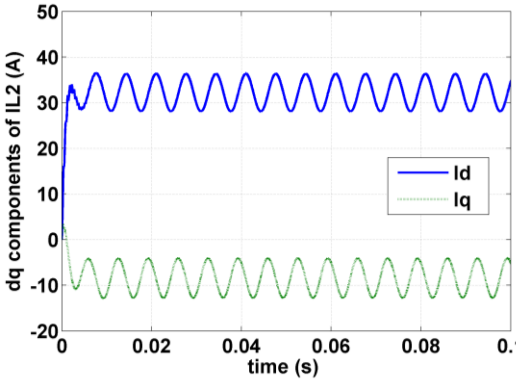

(e) *dq* components of output currents

Fig. 4. Open loop operation of the proposed system in Fig. 2.

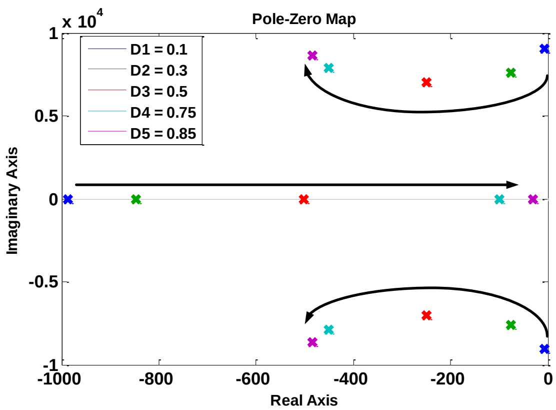

(a) Poles and zeros of G_v

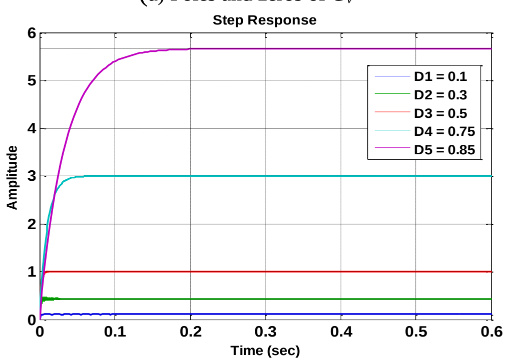

(b) Step Response of G_v

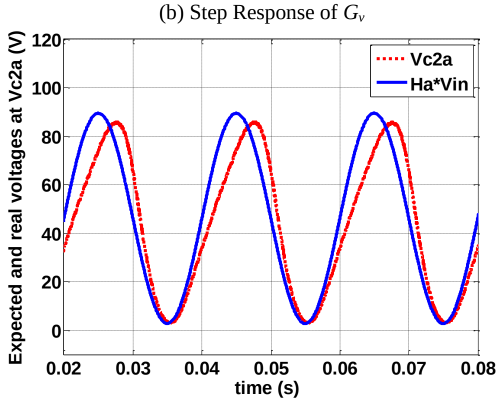

(c) Cuk voltage with time varying duty ratio

Fig. 5. Frequency and time analysis of Cuk Converter

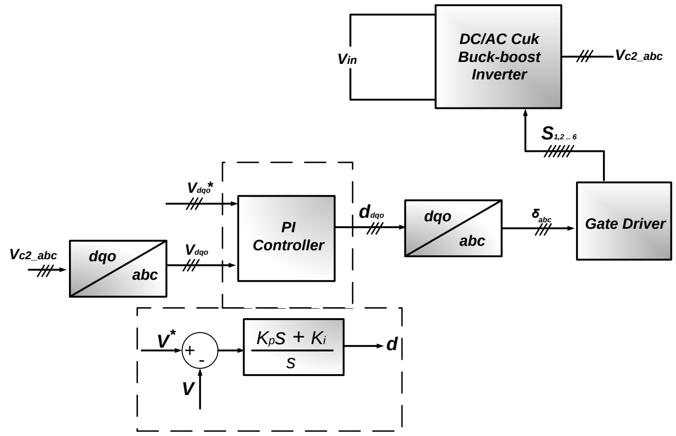

Fig. 6 Control Structure

III. Control Design

The control objective is to track a predefined sinusoidal output voltage. The control structure is shown in Fig. 6. V_d, V_q and V_{dc} are the direct, quadrature, and dc offset components of the output voltage at V_{c2a}, V_{c2b} and V_{c2c}. The subscript '*' refers to a reference value. K_p and K_i are the proportional and integral gains of the PI controller. From equation 3b, the control input is considered the input voltage V_{in}. However, normally, the voltage of the PV is constant over a short period, depending on the MPPT operation, and hence the control input should be written in terms of the time varying duty ratio δ. The small signal equations of the Cuk converter can be driven from equation 3c by considering the small signal deviations $\hat{x}, \hat{y}$ *and* $\hat{u}$ where

$$\begin{aligned} \hat{x} &= x - X \\ \hat{v}_o &= v_o - V_o \\ \hat{d} &= d - D \end{aligned} \tag{7a}$$

X, V_o and D are the steady state values of x, v_o and d

$$\dot{\hat{x}} = a\hat{x} + b\hat{d}$$

$$\hat{v}_o = y\hat{x}$$

$$a = \begin{bmatrix} 0 & \frac{-(1+D)}{L_1} & 0 \\ \frac{(1-D)}{C_1} & 0 & -\frac{D}{C_1} \\ 0 & \frac{D}{L_2} & \frac{-Z}{L_2} \end{bmatrix}, B = \begin{bmatrix} \frac{V_{c1}}{L_1} \\ \frac{-(I_{L1}+I_{L2})}{C_1} \\ \frac{V_{c1}}{L_2} - \frac{Z}{L_2} I_{L2} \end{bmatrix} \tag{7b}$$

$$y = [0 \quad 0 \quad Z], \hat{x} = [\hat{i}_{L1} \quad \hat{v}_{c1} \quad \hat{i}_{L2}]$$

where; V_{c1}, I_{L1} *and* I_{L2} are the steady state values of v_{c1}, i_{L1} *and* i_{L2} respectively

In order to ease the control design process, a point at the middle of the trajectory in Fig. 5a, where $d = 0.5$, is chosen to be an intermediate operating point. The poles loci of the closed loop system of (7b) are plotted in two different ways. In Fig. 7a, K_i is held constant at 0.7 and K_p is varied in the range [0.1:0.8]. Similarly, Fig. 7b shows K_p held constant and K_i varied from [0.1:0.8]. From Fig. 7a, increasing the proportional value drives the poles toward the right hand side. From Fig. 7b, the imaginary poles are locked in their loci

This article has been accepted for publication in a future issue of this journal, but has not been fully edited. Content may change prior to final publication. Citation information: DOI 10.1109/JESTPE.2014.2313185, IEEE Journal of Emerging and Selected Topics in Power Electronics

while the real poles move away from the origin to the left hand side. The gain values are selected by compromising between both cases. From Fig. 7a and 7b, selecting K_p = 0.3 and K_i = 0.4 provides preliminary proper dynamic performance and stability margin from the imaginary axis.

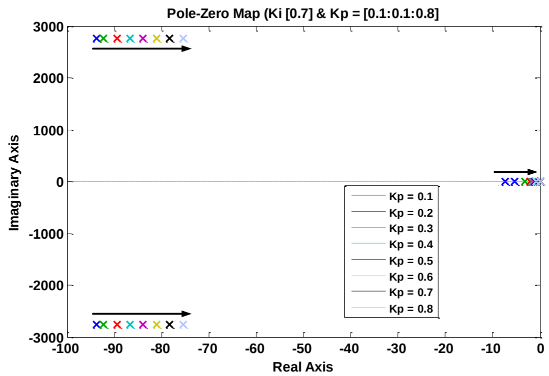

(a) Pole-zero map of (7b) when K_i is held constant at (0.7) and K_p is varied in [0.1:0.8].

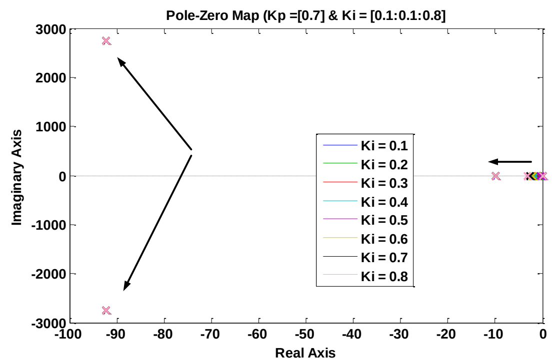

(b) Pole-zero map of (7b) when K_p is held constant at (0.1) and K_i is varied in [0.1:0.8].

Fig. 7. Root loci for a fixed K_i and a range of K_p or vice versa.

The proposed three-phase Cuk inverter is simulated firstly using MATLAB/SIMULINK with the selected parameters and gain values. Fig. 8 shows the results for the voltage response. The reference values are set to build three-phase output voltages of 100V peak-to-peak with 50V dc-offset. V_d, V_q and V_o are set to 50V, 0V and 50 V respectively, to fulfill the rated values of Table. I. However the *dq* components in Fig. 8b show that the actual output voltages and currents still have second harmonic components. This can be elucidated by the nonlinear nature of the Cuk converters as described. Fig. 8c and 8d show the output three-phase current and its 2nd order harmonic components. The input dc current and its 50 kHz ripple are shown in Fig. 8e. By increasing the Cuk converter parameters (L_1, L_2 and C_1), the trajectory of the poles in Fig. 5a becomes shorter. Hence, the effect of Cuk nonlinearity decreases and the 2nd order harmonic decreases in the output currents and voltages. However, increasing the converter parameters will affect the size, cost, losses and will add to the control complexity. A solution is proposed in Fig 9 where the controller is modified with a band pass filter tuned at the 2nd harmonic, 3rd harmonic within the *dq* frame, to extract its components in the output voltage. The filter's transfer function is stated in (8a) where f_b is the center frequency and a is selected to adjust the filter's band width to cater for a $\pm$1% frequency variation. A proportional-resonant (PR) controller is inserted to force this component to equal zero. The PR controller transfer function is shown in (8b), which gives a high gain at a certain angular frequency ω_o enabling the control of this frequency component. The values of PR controller are chosen to be small so as not to interrupt the main PI loop. Fig. 10 shows the minor impact of the new PR-controller on the main control loop with gain values K_{pr} = 0.1 and K_{rr} = 40. The results are shown in Fig. 11 where the PR controller is able to suppress the 2nd harmonic components from the voltages and currents.

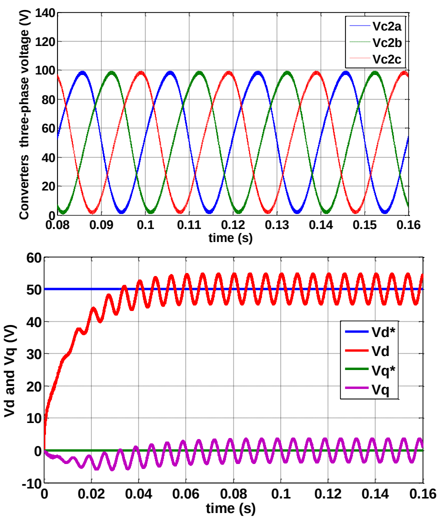

(a) Output voltages at V_{c2a}, V_{c2b} and V_{c2c} and corresponding *dq* components

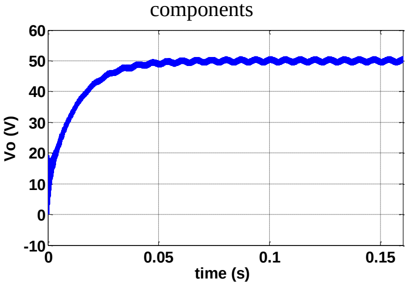

(b) Output voltage dc offset

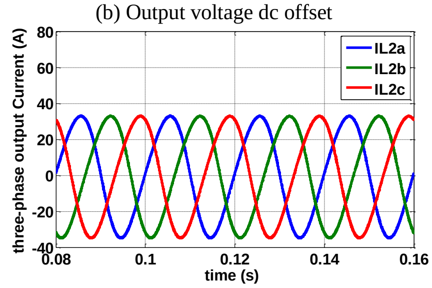

(c) Three-phase output current

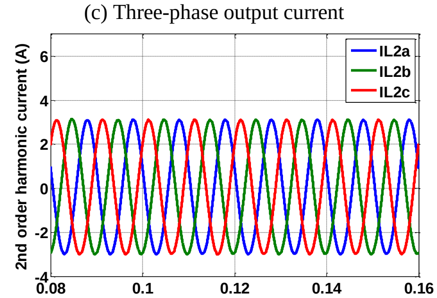

(d) 2nd order harmonic components of three-phase output current

This article has been accepted for publication in a future issue of this journal, but has not been fully edited. Content may change prior to final publication. Citation information: DOI 10.1109/JESTPE.2014.2313185, IEEE Journal of Emerging and Selected Topics in Power Electronics

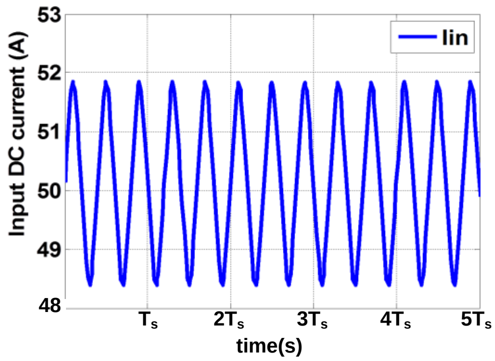

(e) Input DC current

Fig. 8. Proposed system under PI control in Fig. 6

The new $H_{a,\ b\ and\ c}$ ratios shown in Fig. 11e are responsible for eliminating the 2nd order harmonic current in Fig. 11d. In order to suppress the input current ripple, the PWM carrier signals are displaced by 120° as shown in Fig. 12a. In this way, the converters input currents, shown in Fig.12b, charge and discharge in different time periods, instead of all being charged and discharged simultaneously and hence, the high frequency ripple in total input current I_{in} is reduced to 0.6% pp, compared with the symmetric PWM signals shown in Fig. 8e (6% pp). This reduction may alleviate the need for PV output capacitive filtering. Fig. 13 shows the same operation when the proposed system is connected to a voltage source of 250V via a 1:5 step-up transformer under unity power factor operation where I_o = 33.33A and γ=0.

$$G_{bp} = \frac{a\ s}{\frac{1}{(2\pi f_b)^2} s^2 + a\ s + 1} \tag{8a}$$

$$G_{pr} = K_{pr} + \frac{K_{rr}\ s}{s^2 + \omega_o^2},\ \omega_o = 2\pi f \tag{8b}$$

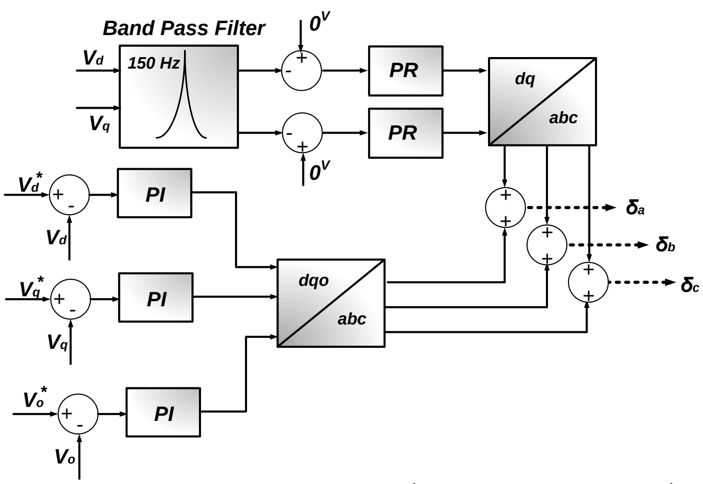

Fig. 9. Control structure with eliminating the 3rd harmonic in the dq frame (2nd in the stationary)

IV. Experimental Results

The prototype in Fig. 14 of three Cuk converters rated as shown in Table. I and controlled with a TMS320F280335 DSP, was used to verify system conception and the presented mathematical analysis. The passive element values are L_1 = 1.014 mH, L_2 = 1.037mH, and C_1 = 10.4 µF. Two IRGP4062DPBF IGBTs have been employed for S_1 and S_2 with their freewheel diodes D_1 and D_2. Fig. 15 shows the proposed system operation when the system is closed loop controlled as shown in Fig. 6. The references are set to constitute three-phase output voltages of 100V peak-to-peak with a 50V dc-offset. V_d, V_q and V_o are set to 50V, 0V and 50V respectively.

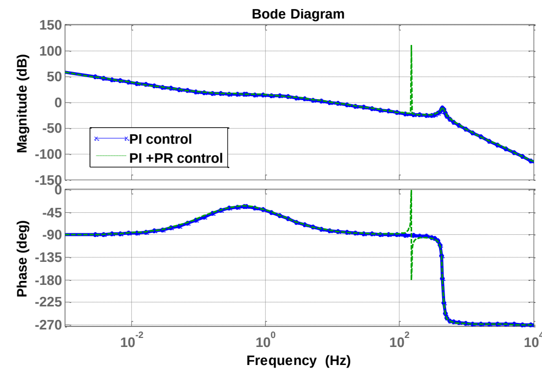

Fig. 10. Impact of the additional control loop

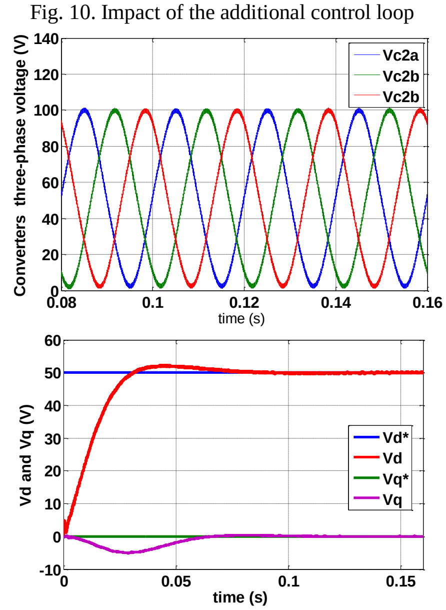

(a) Output voltages at V_{c2a}, V_{c2b} and V_{c2c} and corresponding dq components

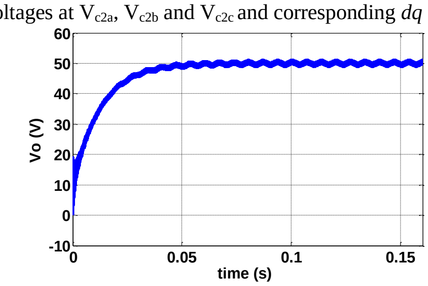

(b) Output voltage dc offset

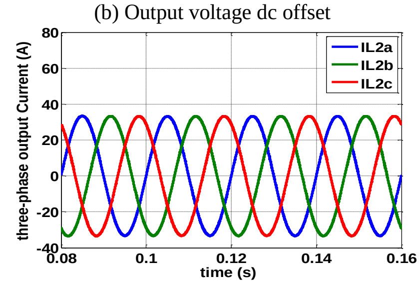

(c) Three-phase output current

This article has been accepted for publication in a future issue of this journal, but has not been fully edited. Content may change prior to final publication. Citation information: DOI 10.1109/JESTPE.2014.2313185, IEEE Journal of Emerging and Selected Topics in Power Electronics

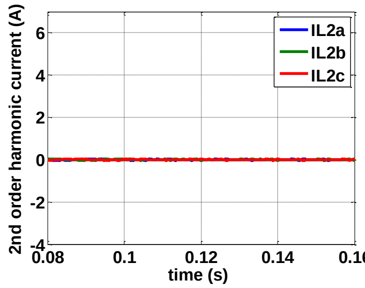

(d) 2nd order harmonic components of three-phase output current

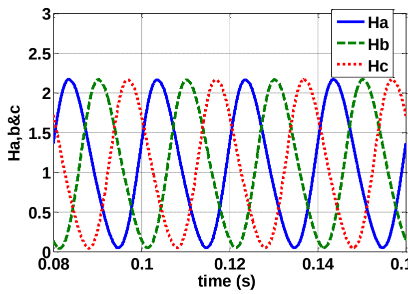

(e) New $H_{a,b,\ and c}$

Fig. 11. Proposed system under PI control in Fig. 9

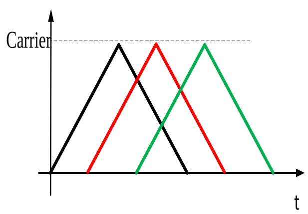

(a) Displaced PWM carrier signals

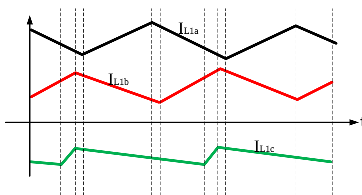

(b) Input Currents $I_{L1a,b,\ and\ c}$

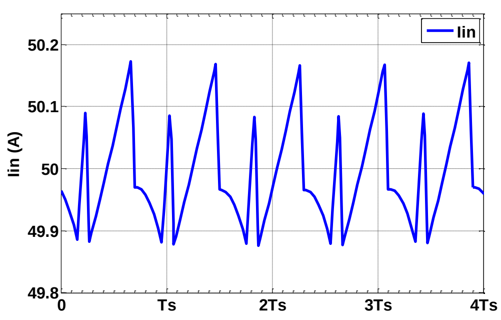

(c) Total Input dc current I_{in}

Fig. 12. Reduced high frequency ripples

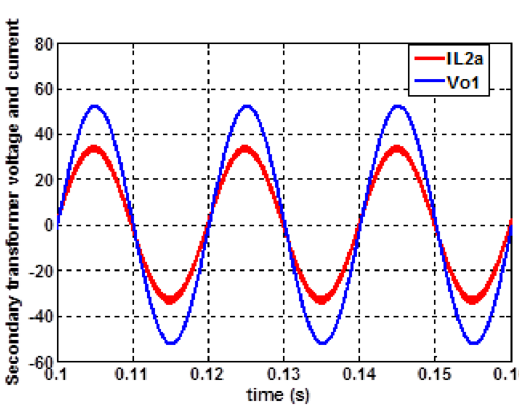

Fig. 13. Secondary voltages and currents

As previously mentioned, the Cuk three-phase voltage and load three-phase current in Fig. 15a, b appear distorted. The input currents I_{L1a}, I_{L1b} and I_{L1c} are shown in Fig. 15c with current ripples ΔI_{L1} and ΔI_{L2} restricted to the acceptable limits in Table. I. The 2nd order harmonic current components are measured with the DSP and plotted in Fig. 15e. The corresponding duty ratios are shown in Fig. 15e and all the results are comparable with the simulations in Fig. 8. The additional PR control loop is inserted then and its effect is shown in Fig. 16 where the Cuk three-phase voltage 2nd order distortion is reduced. Fig. 16c shows the significant reduction of the 2nd order output current component because of the additional control loop. The modified duty ratios are shown in Fig. 16d. The experimental results here verify the simulations in Fig. 11. In order to reduce the input current (I_{in}) ripples, the displaced carrier signals described in Fig. 12a are generated inside the DSP instead of the symmetric PWM mode. The effect on the input current ripples is shown in Fig. 16e where the high frequency ripples are reduced by 90%.Finally, Fig. 17 shows the output voltage and current when the system is connected to the grid via a 1:5 step-up transformer and the result are similar to the computer simulation in Fig. 13. Fig. 18 shows the operation at 0.95 lagging power factor. Detailed overall control analysis, including MPPT operation, as well as the effect of grid side imbalance and low order harmonics are to be considered in future publications

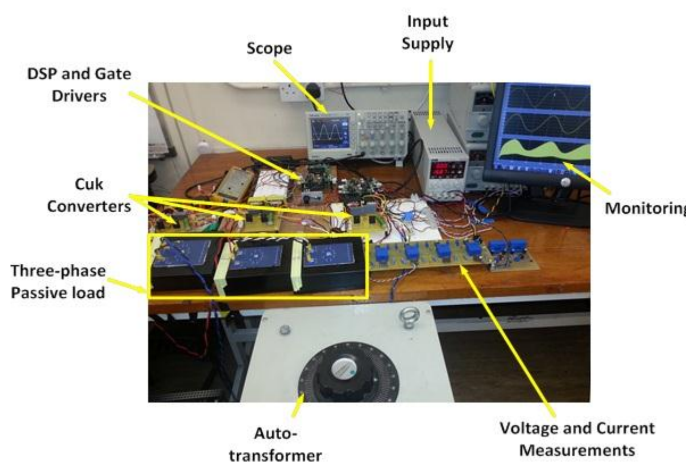

Fig. 14. Experimental prototype

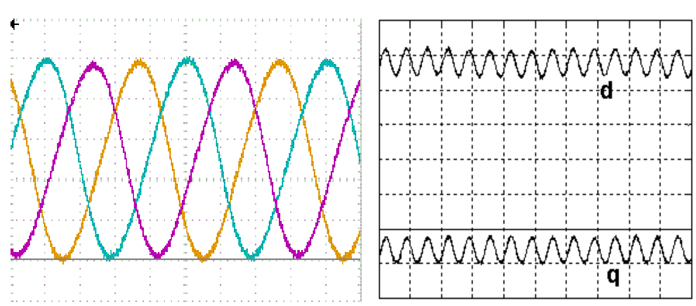

20V/div – 5ms/div 10V/div – 10ms/div

(a) Output voltages at V_{c2a}, V_{c2b} and V_{c2c} and corresponding dq components

This article has been accepted for publication in a future issue of this journal, but has not been fully edited. Content may change prior to final publication. Citation information: DOI 10.1109/JESTPE.2014.2313185, IEEE Journal of Emerging and Selected Topics in Power Electronics

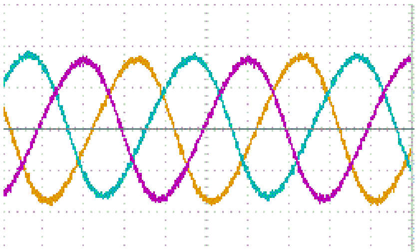

20A/div – 5ms/div
(b) three-phase output current

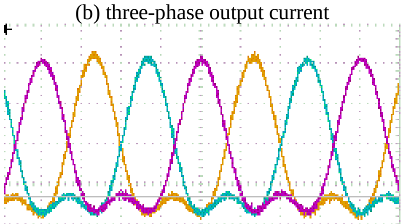

20A/div – 5ms/div
(c) Cuk input currents I_{L1a},I_{L1b} and I_{L1c}

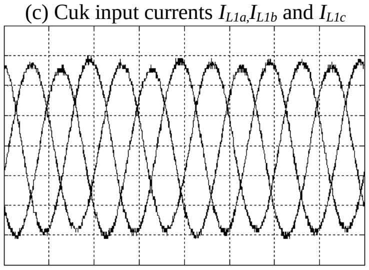

1 A/div – 5ms/div
(d) 2nd order harmonic components of three-phase output current

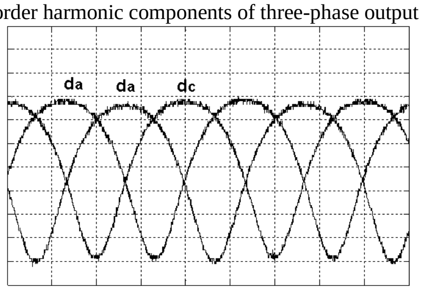

0.1 (s/s)/div – 5ms/div
(e) duty ratios

Fig. 15. Proposed system under PI control in Fig. 6

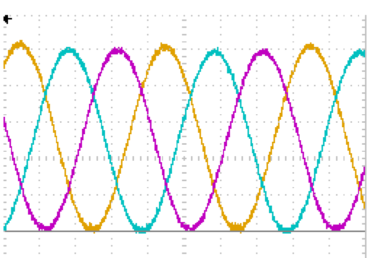

20V/div – 5ms/div

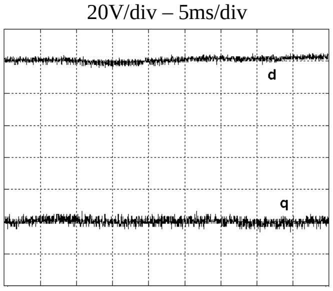

10V/div – 10ms/div
(a) Output voltages at V_{c2a}, V_{c2b} and V_{c2c} and corresponding *dq* components

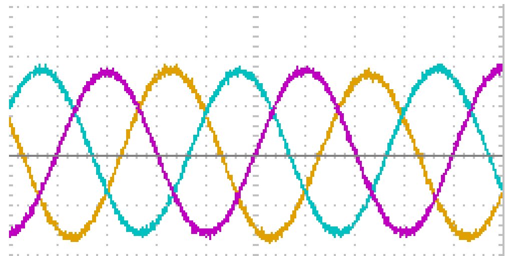

20A/div – 5ms/div
(b) three-phase output current

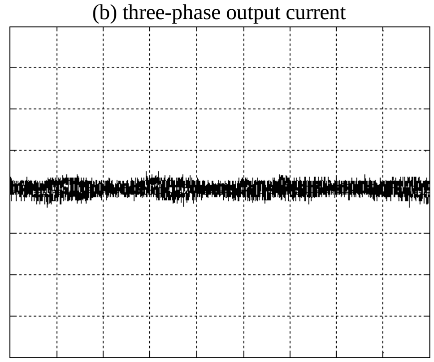

1 A/div – 5ms/div
(c) 2nd order harmonic components of three-phase

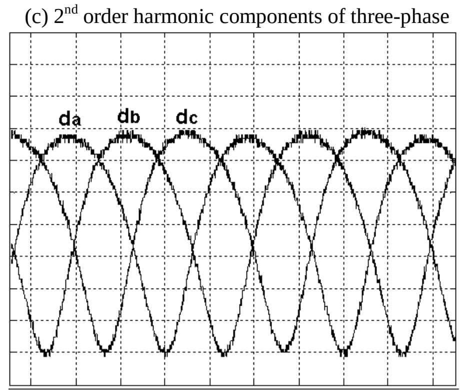

(d) duty ratios

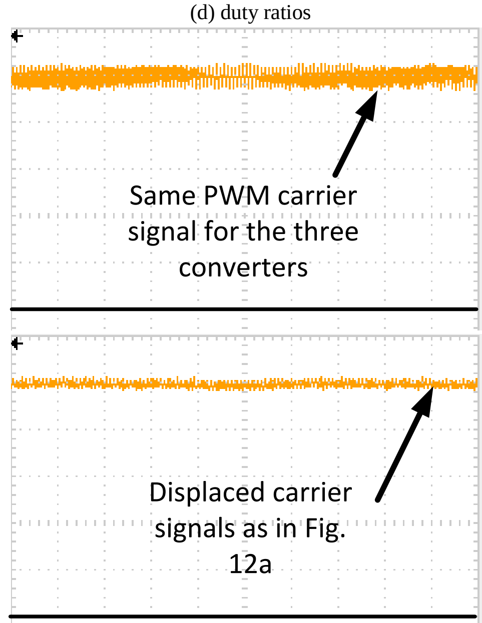

10A/div – 5ms/div
(e) Total input dc current (I_{in})

Fig.16 Proposed system, under PI+PR control in Fig. 9

This article has been accepted for publication in a future issue of this journal, but has not been fully edited. Content may change prior to final publication. Citation information: DOI 10.1109/JESTPE.2014.2313185, IEEE Journal of Emerging and Selected Topics in Power Electronics

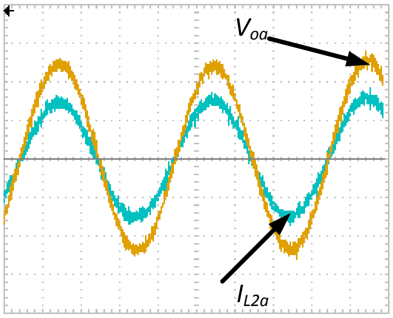

20V/div – 20A/div – 5ms/div

Fig.17. Secondary voltage and currents

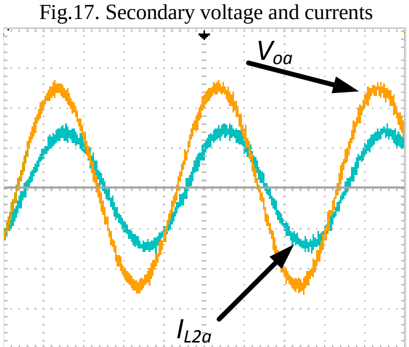

20V/div – 20A/div – 5ms/div

Fig.18. Operation at 0.95 PF

V. CONCLUSION

Due to its inherent current sourcing nature, the Cuk converter is an attractive choice for dc-ac converters in PV applications. The proposed single-stage three-phase Cuk-based inverter introduces several merits when employed for PV applications. Continuous input current enables direct MPPT techniques and the ability of paralleling dc-ac converters at the same PCC promote the proposed converter as viable topology for PV applications. Importantly, because of low input current ripple, no capacitor is required across the PV array (and if used to bypass high frequency switching components, plastic capacitors can be used instead of low reliability electrolytic types). Generally, high order converters like Cuk converters have been avoided in inverter applications because of their control complexity. Moreover, the Cuk converter's inherent nonlinearity is a reason for output current and voltage distortion. The effect of this nonlinearity can be relieved by increasing the Cuk converter inductances and capacitance. However, this adversely affects the total cost, size and control complexity. In this paper, a three-phase dc-ac Cuk converter based current source inverter has been proposed and assessed. The state space averaging method was used to design the control structure. An additional control loop reduced distortion with low passive element values. Satisfactory results in terms of reduced 2^{nd} order harmonic components in the output currents and voltages were obtained and verified by MATLAB/SIMULINK. An inverter system was used to produce experimental results that confirmed system performance. Detailed overall control analysis, including MPPT operation, as well as the effect of grid side imbalance, common mode voltage, and low order harmonics are to be considered in future publications.

ACKNOWLEDGEMENT

This publication was made possible by NPRP grant (NPRP 4-250-2-080) from the Qatar National Research Fund (a member of Qatar Foundation). The statements made herein are solely the responsibility of the authors.

REFERENCES

[1] Boroyevich, D. ; Cvetkovic, I. ; Burgos, R. ; Dong, D.; , "Intergrid: A Future Electronic Energy Network?", Emerging and Selected Topics in Power Electronics, IEEE Journal of, vol.1, no.3, pp. 127-138, Sep. 2013

[2] Kassakian, J.G. ; Jahns, T.M.; , "Evolving and Emerging Applications of Power Electronics in Systems", Emerging and Selected Topics in Power Electronics, IEEE Journal of, vol.1, no.2, pp. 47-58, Jun. 2013

[3] Caceres, R.O.; Barbi, I., "A boost DC-AC converter: analysis, design, and experimentation," *Power Electronics, IEEE Transactions on*, vol.14, no.1, pp.134-141, Jan 1999.

[4] Errabelli, R. R.; Mutschler, P.; , "Fault-Tolerant Voltage Source Inverter for Permanent Magnet Drives," Power Electronics, IEEE Transactions on, vol.27, no.2, pp.500-508, Feb. 2012

[5] Zhang, W.; Hou, Y.; Liu, X.; Zhou, Y.; , "Switched Control of Three-Phase Voltage Source PWM Rectifier Under a Wide-Range Rapidly Varying Active Load," Power Electronics, IEEE Transactions on, vol.27, no.2, pp.881-890, Feb. 2012

[6] Patel, H.; Agarwal, V., "MPPT Scheme for a PV-Fed Single-Phase Single-Stage Grid-Connected Inverter Operating in CCM With Only One Current Sensor," *IEEE Transactions on Energy Conversion,*, vol.24, no.1, pp.256-263, March 2009.

[7] Wei Zhao; Lu, D.D.-C.; Agelidis, V.G., "Current Control of Grid-Connected Boost Inverter With Zero Steady-State Error," *IEEE Transactions on Power Electronics,*, vol.26, no.10, pp.2825-2834, Oct. 2011.

[8] Prasad, B.S.; Jain, S.; Agarwal, V., "Universal Single-Stage Grid-Connected Inverter," *Energy Conversion, IEEE Transactions on*, vol.23, no.1, pp.128-137, March 2008.

[9] Minsoo Jang; Ciobotaru, M.; Agelidis, V.G., "A Single-Phase Grid-Connected Fuel Cell System Based on a Boost-Inverter," *IEEE Transactions on Power Electronics,*, vol.28, no.1, pp.279-288, Jan. 2013

[10] Chunkag, V.; Kamnarn, U., "Parallelling three-phase AC to DC converter using CUK rectifier modules based on power balance control technique," *Power Electronics, IET*, vol.3, no.4, pp.511-524, July 2010.

[11] Knight, J.; Shirsavar, S.; Holderbaum, W., "An improved reliability Cuk based solar inverter with sliding mode control," *IEEE Transactions on Power Electronics,*, vol.21, no.4, pp.1107-1115, July 2006.

[12] J. Kikuchi and T. A. Lipo, "Three-Phase PWM Boost–Buck Rectifiers With Power-Regenerating Capability" IEEE Transactions on Industry Applications, Vol. 38, No. 5, pp. 1361-1369, September/October 2002.

[13] Yaosuo Xue; Liuchen Chang; Sren Baekhj Kjaer; Bordonau, J.; Shimizu, T., "Topologies of single-phase inverters for small distributed power generators: an overview," *IEEE Transactions on Power Electronics*, vol.19, no.5, pp.1305-1314, Sept. 2004.

[14] Quan Li; Wolfs, P., "A Review of the Single Phase Photovoltaic Module Integrated Converter Topologies With Three Different DC Link Configurations," *IEEE Transactions on Power Electronics*, vol.23, no.3, pp.1320-1333, May 2008.

[15] Kadri, R.; Gaubert, J-P; Champenois, G., "Nondissipative String Current Diverter for Solving the Cascaded DC–DC Converter Connection Problem in Photovoltaic Power Generation System," *IEEE Transactions on Power Electronics*, vol.27, no.3, pp.1249-1258, March 2012.

[16] Williams, B.W., "DC-to-DC Converters With Continuous Input and Output Power," *IEEE Transactions on Power Electronics*, vol.28, no.5, pp.2307-2316, May 2013.

[17] Gonzalez, Roberto; Lopez, J.; Sanchis, P.; Marroyo, L., "Transformerless Inverter for Single-Phase Photovoltaic Systems," *IEEE Transactions on Power Electronics*, vol.22, no.2, pp.693-697, March 2007.

[18] Hongrae Kim; Parkhideh, B.; Bongers, T.D.; Heng Gao, "Reconfigurable Solar Converter: A Single-Stage Power Conversion

This article has been accepted for publication in a future issue of this journal, but has not been fully edited. Content may change prior to final publication. Citation information: DOI 10.1109/JESTPE.2014.2313185, IEEE Journal of Emerging and Selected Topics in Power Electronics

PV-Battery System," *IEEE Transactions on Power Electronics*, vol.28, no.8, pp.3788-3797, Aug. 2013.

[19] Prasanna, P.R.; Rathore, A.K., "Analysis, Design, and Experimental Results of a Novel Soft-Switching Snubberless Current-Fed Half-Bridge Front-End Converter-Based PV Inverter," *Power Electronics, IEEE Transactions on* , vol.28, no.7, pp.3219-3230, July 2013.

[20] Darwish, A.; Elserougi, A.; Abdel-Khalik, A.S.; Ahmed, S.; Massoud, A.; Holliday, D.; Williams, B.W., "A single-stage three-phase DC/AC inverter based on Cuk converter for PV application," *GCC Conference and Exhibition (GCC), 2013 7th IEEE* , vol., no., pp.384,389, 17-20 Nov. 2013

[21] Chung, H.S.-H.; Tse, K. K.; Hui, S.Y.R.; Mok, C. M.; Ho, M. T., "A novel maximum power point tracking technique for solar panels using a SEPIC or Cuk converter," *Power Electronics, IEEE Transactions on* , vol.18, no.3, pp.717-724, May 2003.

[22] Himmelstoss, F.A.; Walter, C. M., "A simple cuk converter derivated two-quadrant DC motor controller," *Power Electronics Electrical Drives Automation and Motion (SPEEDAM), 2010 International Symposium on* , vol., no., pp.1108-1112, 14-16 June 2010.

Ahmed Darwish received the B.Sc. and M.Sc. degrees in electrical engineering from the faculty of engineering, Alexandria University, Egypt, in 2008 and 2012, respectively. From 2009 to 2012, he was a research associate at Texas A&M University at Qatar. He is currently pursuing his PhD studies in Electric and Electronic Engineering Department at the University of Strathclyde, Glasgow, UK. His research interests include dc-dc converters, multi-level converters, electric machines, digital control of power electronic systems, energy conversion, renewable energy, and power quality.

Derrick Holliday has research interests in the areas of power electronics, electrical machines and drives. In 1995 he obtained the degree of PhD from Heriot Watt University and, since then, has held full-time academic posts at the Universities of Bristol and Strathclyde. He has authored or co-authored over 70 academic journal and conference publications. He is currently leading industrially funded research in the field of power electronics for HVDC applications, and is co-investigator on research programmes in the fields photovoltaic systems and the interface of renewable energy to HVDC systems.

Shehab Ahmed (SM'12) was born in Kuwait City, Kuwait in July 1976. He received the B.Sc. degree in Electrical Engineering from Alexandria University, Alexandria, Egypt, in 1999; the M.Sc. and Ph.D. degrees from the Department of Electrical & Computer Engineering, Texas A&M University, College Station, TX in 2000 and 2007, respectively. From 2001 to 2007, he was with Schlumberger Technology Corporation workinn downhole mechatronic systems. He is currently an Assistant Professor with Texas A&M University at Qatar, Doha, Qatar. His research interests include mechatronics, solid-state power conversion, electric machines, and drives.

Ahmed M. Massoud (SM’11) received the B.Sc. (first class honors) and M.Sc. degrees from the Faculty of Engineering, Alexandria University, Egypt, in 1997 and 2000, respectively, and the Ph.D. degree in electrical engineering from the Computing and Electrical Department, Heriot-Watt University, Edinburgh, U.K., in 2004. From 2005 to 2008, he was a Research Fellow at Strathclyde University, Glasgow, U.K. From 2008 to 2009, he was a Research Fellow at Texas A&M at Qatar, Doha, Qatar. From 2009 to 2012, he was an Assistant Professor at the Department of Electrical Engineering, College of Engineering, Qatar University, where he is currently an Associate Professor in the same department. His research interests include Power Electronics, Energy Conversion, Renewable Energy and Power Quality.

B.W. Williams received the M.Eng.Sc. degree from the University of Adelaide, Australia, in 1978, and the Ph.D. degree from Cambridge University, Cambridge, U.K., in 1980. After seven years as a Lecturer at Imperial College, University of London, U.K., he was appointed to a Chair of Electrical Engineering at Heriot-Watt University, Edinburgh, U.K, in 1986. He is currently a Professor at Strathclyde University, UK. His teaching covers power electronics (in which he has a free internet text) and drive systems. His research activities include power semiconductor modelling and protection, converter topologies, soft switching techniques, and application of ASICs and microprocessors to industrial electronics.